



UNIVERSIDAD DE INVESTIGACIÓN DE TECNOLOGÍA EXPERIMENTAL YACHAY

Escuela de Ciencias de la Tierra, Energía y Ambiente

TÍTULO: SUBSURFACE WATER FLOW ASSESSED WITH ELECTRICAL RESISTIVITY AND GROUND-PENETRATING RADAR IN YACHAY TECH, ECUADOR

Trabajo de integración curricular presentado como requisito
para la obtención del título de Geóloga

Autor:

ARTEAGA POZO MARÍA EMILIA

Tutor:

PIISPA ELISA JOHANNA

Urcuquí, Agosto del 2019

Urcuquí, 30 de agosto de 2019

SECRETARÍA GENERAL
(Vicerrectorado Académico/Cancillería)
ESCUELA DE CIENCIAS DE LA TIERRA, ENERGÍA Y AMBIENTE
CARRERA DE GEOLOGÍA
ACTA DE DEFENSA No. UITEY-GEO-2019-00002-AD

En la ciudad de San Miguel de Urcuquí, Provincia de Imbabura, a los 30 días del mes de agosto de 2019, a las 09:00 horas, en el Aula AI-101 de la Universidad de Investigación de Tecnología Experimental Yachay y ante el Tribunal Calificador, integrado por los docentes:

<u>Presidente Tribunal de Defensa</u>	<u>Dra. FOSTER ANNA , Ph.D.</u>
<u>Miembro No Tutor</u>	<u>Dr. CARRILLO ALVAREZ, EMILIO , Ph.D.</u>
<u>Tutor</u>	<u>Dra. PIISPA , ELISA JOHANNA , Ph.D.</u>

Se presenta el(la) señor(ita) estudiante **ARTEAGA POZO, MARIA EMILIA**, con cédula de identidad No. **1723065650**, de la **ESCUELA DE CIENCIAS DE LA TIERRA, ENERGÍA Y AMBIENTE**, de la Carrera de **GEOLOGÍA**, aprobada por el Consejo de Educación Superior (CES), mediante Resolución **RPC-SE-10-No.031-2016**, con el objeto de rendir la sustentación de su trabajo de titulación denominado: **Subsurface Water Flow Assessed with Electrical Resistivity and Ground-Penetrating Radar in Yachay Tech, Ecuador.**, previa a la obtención del título de **GEÓLOGO/A**.

El citado trabajo de titulación, fue debidamente aprobado por el(los) docente(s):

Tutor Dra. PIISPA , ELISA JOHANNA , Ph.D.


Y recibió las observaciones de los otros miembros del Tribunal Calificador, las mismas que han sido incorporadas por el(la) estudiante.


Previamente cumplidos los requisitos legales y reglamentarios, el trabajo de titulación fue sustentado por el(la) estudiante y examinado por los miembros del Tribunal Calificador. Escuchada la sustentación del trabajo de titulación, que integró la exposición de el(la) estudiante sobre el contenido de la misma y las preguntas formuladas por los miembros del Tribunal, se califica la sustentación del trabajo de titulación con las siguientes calificaciones:

Tipo	Docente	Calificación
Presidente Tribunal De Defensa	Dra. FOSTER ANNA , Ph.D.	9.4
Miembro Tribunal De Defensa	Dr. CARRILLO ALVAREZ, EMILIO , Ph.D.	9.1
Tutor	Dra. PIISPA , ELISA JOHANNA , Ph.D.	9.4

Lo que da un promedio de: **9.3 (Nueve punto Tres)**, sobre 10 (diez), equivalente a: **APROBADO**

Para constancia de lo actuado, firman los miembros del Tribunal Calificador, el/la estudiante y el/la secretario ad-hoc.


ARTEAGA POZO, MARIA EMILIA
Estudiante


Dra. FOSTER ANNA , Ph.D.
Presidente Tribunal de Defensa


Dra. PIISPA , ELISA JOHANNA , Ph.D.
Tutor

Dr. CARRILLO ALVAREZ, EMILIO , Ph.D.
Miembro No Tutor

TERÁN ROSALES, ANDREA YOLANDA
Secretario Ad-hoc

AUTORÍA

Yo, **María Emilia Arteaga Pozo**, con cédula de identidad 1723065650, declaro que las ideas, juicios, valoraciones, interpretaciones, consultas bibliográficas, definiciones y conceptualizaciones expuestas en el presente trabajo; así cómo, los procedimientos y herramientas utilizadas en la investigación, son de absoluta responsabilidad de el/la autora (a) del trabajo de integración curricular. Así mismo, me acojo a los reglamentos internos de la Universidad de Investigación de Tecnología Experimental Yachay.

Urcuquí, Agosto del 2019



María Emilia Arteaga Pozo
CI: 1723065650

AUTORIZACIÓN DE PUBLICACIÓN

Yo, **María Emilia Arteaga Pozo**, con cédula de identidad 1723065650, cedo a la Universidad de Tecnología Experimental Yachay, los derechos de publicación de la presente obra, sin que deba haber un reconocimiento económico por este concepto. Declaro además que el texto del presente trabajo de titulación no podrá ser cedido a ninguna empresa editorial para su publicación u otros fines, sin contar previamente con la autorización escrita de la Universidad.

Asimismo, autorizo a la Universidad que realice la digitalización y publicación de este trabajo de integración curricular en el repositorio virtual, de conformidad a lo dispuesto en el Art. 144 de la Ley Orgánica de Educación Superior

Urcuquí, Agosto del 2019.



María Emilia Arteaga Pozo
CI: 1723065650

ACKNOWLEDGEMENTS

I would like to thank my advisor Elisa Piispa for helping me finish my undergraduate thesis and for motivate me all the time even when things went wrong. I have learnt how to develop a research project and deal with problems. Thanks to my co-advisors too: Celine Mandon, Luis Pineda and, Eva Sutter who always had time to talk with me to share ideas and work in the field and in the lab.

I would like to acknowledge all my friends (Bryan Chamba & Gisella Pilliza and mosquitos) that worked with me in the field, being hungry, hot and tired. I would not have achieved it without you.

Finally, but not least, thank you to my family which have support me in every step of my degree in Science, all the love has result in a beautiful fruit of this tree we took care together.

ABSTRACT

Water management plays an important role in supplying populations with clean water for agriculture, livestock and human consumption. Hence, investigation of the quality of aquifers, watercourses and their potential pollutants is important for communities all over the world. Here, we used electrical resistivity and ground-penetrating radar, which have been utilized successfully for water flow assessment, to evaluate a possibly contaminated open water-storage pool in an emerging city of Yachay in northern Ecuador. In this thesis we compared the subsurface electrical resistivity pseudosections with the radargrams and used physicochemical analysis of water to answer the following questions: (1) Is the water channelled to the pool or is the water channel broken, seeping and causing the vegetation patches around the pool? (2) How is the water flowing at the subsurface below and above the pool? (3) How is this flow being influenced by weather conditions? (4) Is the pool itself in good condition and retaining the water or is there leakage from the pool? (5) Is the water that is flowing through the channel contaminated by pollution or organic waste? The geophysical survey results from 2017 showed that the areas with low resistivity values and high reflectance match with the dense vegetation on the surface. This clearly showed that the channel to the pool was either blocked or broken, creating a distinct leakage pattern around the pool. After 2017 a small channel was dug to the pool again allowing the water to flow again. Monthly electrical resistivity measurements between October 2018 – February 2019 revealed that the subsurface water content shows fluctuations with areal precipitation. The physicochemical and biochemical analysis showed that the water flowing through the ditch is not suitable for human consumption due to its elevated content of BOD and coliforms. However, these values are below the lower limit of greywater and therefore the water is suitable for agriculture and livestock usage.

KEYWORDS

Electrical resistivity, ground-penetrating radar, two-dimensional inversion, groundwater monitoring

RESUMEN

El manejo de agua desempeña un papel importante cuando se suministra agua limpia a las poblaciones para la agricultura, la ganadería y el consumo humano. Por lo tanto, investigaciones sobre la calidad de los acuíferos, los cursos de agua y sus posibles contaminantes son importantes para las comunidades de todo el mundo. Aquí, utilizamos resistividad eléctrica y un radar de penetración del suelo, que se han utilizado con éxito para apreciar flujos de agua, para evaluar una piscina de almacenamiento de agua abierta posiblemente contaminada en una ciudad emergente, Yachay, en el norte de Ecuador. En esta tesis, comparamos modelos de resistividad eléctrica con los radargramas y utilizamos análisis biofísicoquímicos para responder las siguientes preguntas: (1) ¿Se canaliza el agua hacia la piscina o está roto el canal, filtrando y causando los parches de vegetación alrededor de la piscina? (2) ¿Cómo fluye el agua en el subsuelo por debajo y por encima de la piscina? (3) ¿Cómo está influenciado este flujo por las condiciones climáticas? (4) ¿Está la piscina en sí en buenas condiciones y reteniendo el agua o hay fugas en la piscina? (5) ¿El agua que fluye a través del canal está contaminada por desechos orgánicos? Los resultados del estudio geofísico de 2017 mostraron que las áreas con bajos valores de resistividad y alta reflectancia coinciden con la densa vegetación en la superficie. Esto mostró claramente que el canal hacia la piscina estaba bloqueado o roto, creando un patrón de fuga distinto alrededor de la piscina. Después de 2017, se excavó un pequeño canal hacia la piscina, lo que permitió que el agua fluyera nuevamente. Las mediciones mensuales de resistividad eléctrica entre octubre de 2018 y febrero de 2019 revelan que el contenido de agua debajo de la superficie muestra fluctuaciones con la precipitación del área. El análisis físicoquímico y bioquímico muestra que el agua que fluye a través de la zanja no es adecuada para el consumo humano debido a su alto contenido de DBO y coliformes. Sin embargo, estos valores están por debajo del límite inferior de las aguas grises y, por lo tanto, el agua es adecuada para el uso agrícola y ganadero.

PALABRAS CLAVE

Resistividad eléctrica, Radar de penetración del suelo, inversión bi-dimensional, monitoreo de agua subterránea

Table of Contents

AUTORÍA	iv
AUTORIZACIÓN DE PUBLICACIÓN	v
ACKNOWLEDGEMENTS	vi
ABSTRACT	vii
RESUMEN	viii
1 INTRODUCTION	1
2 STATEMENT OF THE PROBLEM	2
3 OBJECTIVES	4
4 METHODS	4
4.1 Stratigraphy Sections	4
4.2 Water Biophysicochemical Analyses	4
4.3 Ground-Penetrating Radar	5
4.3.1 Theory.....	5
4.3.2 Measurement procedure.....	6
4.4 Electrical Resistivity	9
4.4.1 Theory.....	9
4.4.2 Measurement procedure and data analyses	11
5 RESULTS AND DISCUSSION	15
5.1 Stratigraphy of the area	15
5.2 Water Biophysicochemical Analysis	16
5.3 Ground-Penetrating Radar	18
5.4 Electrical Resistivity	19
5.5 Comparison between ER, GPR and stratigraphy	25
6 CONCLUSIONS AND RECOMMENDATIONS	26
7 REFERENCES	27

1 INTRODUCTION

Ecuadorian villages commonly use irrigation ditches (acequias i.e. community operated watercourses) to acquire water for agriculture, livestock and human consumption. This technique had already been applied by our pre-Columbian cultures because they are easy to build and maintain. These irrigation systems helped to expand the territory destined for agriculture in the highlands, transformed deserts into growing areas at the coast and defended the crops against drought (Ribeiro, 2013). In the Ecuadorian Andes, acequias were constructed with traditional technology. Generally, they have a rectangular form because it is believed that the water runs faster that way. They are typically constructed above a tuff bed due to its low permeability. Farmers can use the water throughout the year. They "throw" it to their orchards instead of breaking the bank of the ditch using a metal door which facilitates this process (Knapp, 1988). Even currently, porosity and percolation capacity are things communities need to take into account when planning for the locations of the water storage pools and the acequias.

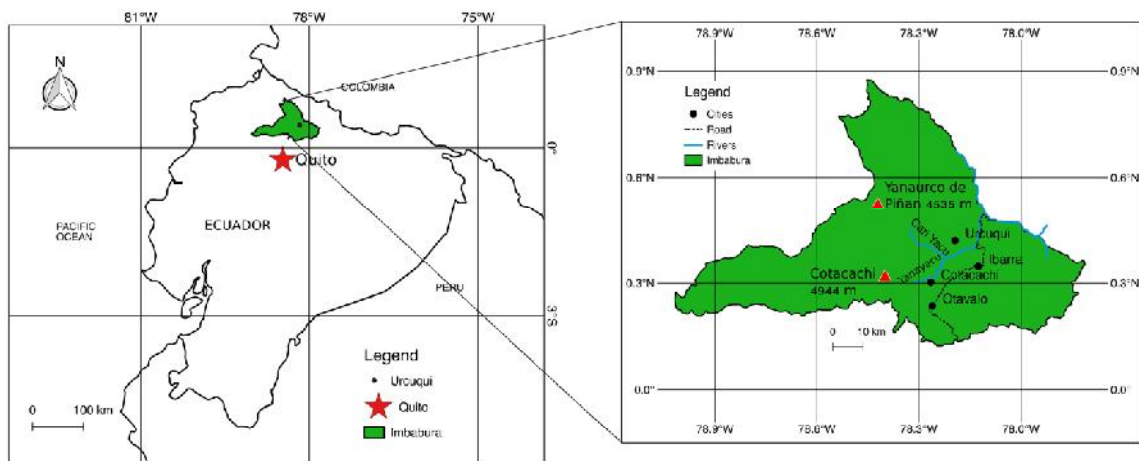


Figure 1. Geographic and topographic relief maps of the study area. On the left is the geographic map of Ecuador with the Imbabura province marked as green. On the right is a close-up showing various cities in the Inter-Andean valley, such as Urququi, the nearest village from Yachay Tech where the pool is located. Also, the distributary rivers and the Cuicocha and Piñan lakes are shown indicating the source regions of the rivers.

Yachay Tech University is the heart of the City of Knowledge Yachay located 2 km from Urququi village, Imbabura, Ecuador (Figure 1). It is located in the Northern Sub-Andean zone surrounded by the Western and Eastern Cordillera. The Juntas de Agua de la “Acequia Jijona” and “Acequia Chiquita” affirm that there are two acequias that provide water to Urququi and Yachay: Jijona and Chiquita. Jijona irrigation ditch comes from Yanayacu River, Pichambiche River, Fucuna Guayco Ravine and Yanayacu Pools. The total irrigation flow is approximately 280 L/s of which 163.5 L/s goes directly to Yachay. The water corresponding to this ditch has a bad smell probably because of

wastewater, garbage or solid waste. However, the quality of the water flowing through this ditch has not been addressed and is only used for agricultural irrigation. Chiquita irrigation ditch comes from Rio Cari Yacu and Herraduras Ravine (Figure 1). Its flow is approximately 620 L/s of which Yachay receives 310.5 L/s. This water is not contaminated and is used as drinking water. The first irrigation ditch described, Jijona, arrives to our study area. The water is supposed to flow into an open water storage pool located near the university buildings at Yachay Tech. The quality of the water in the channel or in the pool has not been tested before. Furthermore, no studies have looked at the water pattern above or below this pool, that would potentially give us indications of the quality or existence of the water channel and the potential leakages from the pool. There are multiple geophysical methods that allow people to plan and to monitor the water flow at the subsurface, but in this research, we will concentrate on two main methods: electrical resistivity tomography (ERT) and ground-penetrating radar (GPR).

ERT method is widely used to define underground structures, the depth of the water table and underground water contamination (Adepelumi et al., 2001; Benson et al., 1997; Park et al., 2016; Simyrdanis et al., 2018; Soupios et al., 2007; Urish, 1983). For example, Abidini et al. (2015) used electrical resistivity survey to investigate potentially problematic zones due to groundwater seepage, similar to the problem we address in this thesis. The same ERT method was used in Syria to demonstrate the origin of water leakages in a dam located in a basin by Al-Fares (2011). GPR method provides significant resolution and excellent sensitivity to variations in pore fluid content and lithology which are often accompanied by fissures and fractures (Sonkamble et al., 2014). Its applications include soil water content (i.e. Bowling et al., 2005, Huisman et al., 2003), archeological investigations (i.e. Dick et al., 2017; Liu et al., 2018), leak detection (i.e. Cataldo et al., 2014; Ramirez et al., 2009) bedrock mapping, karst evaluation, mapping faults and fractures, snow, ice and glaciers (i.e. Feiger et al., 2018), among others. Specifically related with this thesis is the study of Bowling et al. (2005), where the authors delineated fluvial aquifer heterogeneities and distribution of preferential flow paths. Both GPR and ERT methods are non-invasive, since there is no need for drilling or managing wells. They are suitable and easy ways for detecting the structures and underground moisture profile.

2 STATEMENT OF THE PROBLEM

Yachay Tech Campus has a small pool (~65 m by ~25 m) that is supposed to collect water for irrigation purposes. It collects water from Jijona irrigation ditch coming from Yanayacu River. The pool is near the principal path for students, teachers and general public that commutes between the dorms and the other university buildings containing the library, classrooms and restaurant (Figure 2). Since 2015, this pool has experienced different stages. At the beginning of the year mentioned, the pool was totally empty. By September 2015, the pool was full of water. Then again, in 2017 it was empty. As of September 2018, it was completely filled by water transported by a

new superficial channel dug in the ground. Empresa Pública Yachay (Yachay EP), the public company that is in charge of building the university, does not have or share information related to this pool.

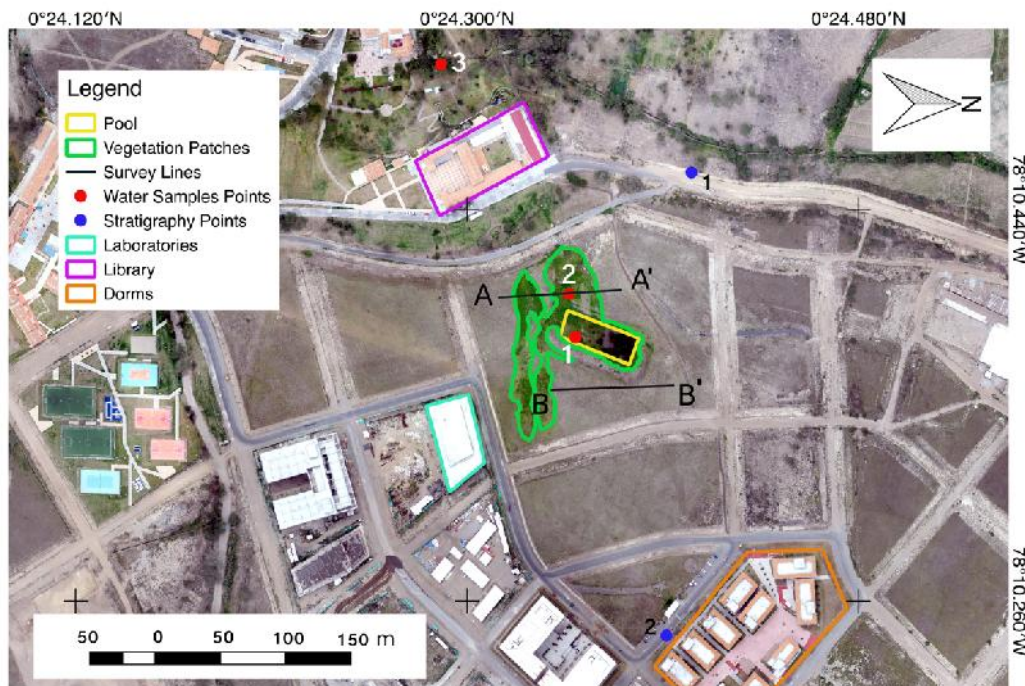


Figure 2. Map of the study area. The patch of vegetation around the pool is shown in green, the pool in yellow, the A-A' and B-B' survey lines in black. Also, the location for stratigraphy sections (purple dots) and water sampling locations (red dots) are shown.

We decided to study the area in December 2017 by implementing ERT and GPR geophysical methods across two survey lines: one located upslope and west above the pool (A - A', Figure 2) and the other downslope and east below the pool (B - B', Figure 2). Our study of two ERT pseudosections with a depth of approximately three meters and two radargrams with a depth of approximately six meters, revealed that: (1) there probably is no water table present in the upper zone; (2) the zones with less resistivity match with the zones with green vegetation; (3) there possibly is a blocked or broken pipeline, that is not transporting water to the pool at all, but instead is leaking and forming these big patches of vegetation on both sides around the pool.

Since our questions were not completely answered the research was resumed in October 2018 in order to know: (1) Is the water flowing into this pool being filtered to its surroundings?; (2) Is all of the water now flowing to the pool through the ditch or is the small ditch also continuing to leak on the field?; and (3) How is this flow related to climatological variations implying solely a natural source?; (4) Are there pathogens, bacteria or any other harmful substances in the water? If this last point is true, it might indicate some of the waters come from the University buildings. For this, we will take into account that: *“Greywater contains soap, shampoo, toothpaste, shaving cream, laundry detergents, hair, lint, body oils, dirt, grease, fats and urine, and the blackwater is a mix of urine, feces and flush water”* (World Health Organization, 2006). These can

be detected with simple chemical analysis such as BOD5, coliforms, total suspended solids, etc. It is important to know the quality of the water in the pool since it is used for irrigation of plants and crops around the city of Yachay.

3 OBJECTIVES

The main research objectives are: (1) Is the water channelled to the pool or is the water channel either blocked or broken, seeping and thereby causing the vegetation patches around the pool? (2) How is the water flowing at the subsurface E (below) and W (above) of the pool? (3) How is this flow being influenced by weather conditions like precipitation, sunny days and cloudy days (4) Is the pool itself in good condition and retaining the water, or is there leakage from the pool? (5) Finally, is the water flowing through the channel contaminated by pollution or organic waste?

4 METHODS

In order to assess the research goals, we planned the following set-up: (a) to observe, analyze and detail the stratigraphy of the area from the nearby road-cuts and utility diggings; (b) to determine if the water flowing through the channel and in the pool is contaminated; (c) to set-up two survey lines for GPR and ERT: both with SN direction (Figure 2); (d) to compare the GPR data, which can reveal the underlying strata and the starting depth of the moisture, with the monthly ERT pseudosections; (e) to observe the climatological data provided by Meteoblue (2019) to infer if the ERT data as a humidity proxy reveals an influence of rainfall data.

4.1 Stratigraphy Sections

To obtain the stratigraphy of the area we took as reference two main locations (Figure 2). The first point is located 150 m away in the upper right zone of the hill. The outcrop can be seen at the left of the road. The second point is 220 m downhill next to the dorms. The outcrop was analyzed when machinery dug a tunnel to place water pipes. Nowadays it is totally covered with asphalt. The thicknesses of the beds were measured with a measuring tape, the diameters of the little clast were measured with a ruler and the sediments were deciphered with a geotechnical gauge.

4.2 Water Biophysicochemical Analyses

In order to analyze the microbiological, physical and chemical properties of the water, we took samples from three specific locations (Figure 2) and did the following analyses:

- 1) Biochemical Oxygen Demand (BOD, also called food for the biomass) is the amount of dissolved oxygen required by aerobic biological organisms to modify organic material existing in a water sample at defined temperature over a

specific time period. In this project, the samples were in incubation for 5 days at 20 °C and the results are in milligrams of oxygen consumed per liter.

- 2) Nitrogen Total Kjeldahl (NTK) is a method to quantify the amount of nitrogen present in organic substances plus the nitrogen contained in the inorganic compounds: ammonia and ammonium ($\text{NH}_3/\text{NH}_4^+$). Nitrate, is not included in this measurement.
- 3) pH is a measurement used to determine the level of acidity or alkalinity of a substance. It has its own scale ranging from zero to fourteen. Zero signifies acid and fourteen alkaline. The pH can be measured by litmus paper or by a pH-meter. In this work, we used the second method.
- 4) Conductivity is a measure of the material's capacity to transfer electric current (Table 1) based on the concentration of dissolved solids substances such as salts. The more ions the more conductive the water is.
- 5) Total suspended particles (TSP), in g/L, is a measure of all inorganic and organic substances present in a liquid as suspended particles. In this project, we used a 0.45 μm membrane to measure the solids in solution.
- 6) Coliforms represent bacteria that are found in the digestive tracts of animals, including humans. They are measured in NMP/100 mL and are analyzed from animals' wastes, plants and soil material.

Table 1. Table of relative dielectric constants, conductivities and electromagnetic wave velocities for a range of geological materials (Reynolds, 1997).

Material	Dielectric constant ϵ_r	Conductivity σ [mS/m]	Electromagnetic wave velocity v [mm/ns]	Resistivity ρ [Ω m]
Air	1	0	300	$\sim 2 \times 10^{16}$
Water (fresh)	81	0.5	33	2
Water (sea)	81 – 88	3000	33	3.3×10^{-5}
Dry Sand	3 – 6	$10^{-4} - 1$	122 – 173	$10^{-4} - 1$
Wet Sand	10 – 32	0.1 – 10	53 – 95	0.1 – 10
Unsaturated Silt	2.5 – 5	1 – 100	134 – 190	0.01 – 1
Saturated Silt	22 – 30	< 100	55 – 64	< 0.01
Dry Clay	2 – 5	2 – 100	134 – 212	0.01 – 0.5
Wet Clay	8 – 40	20 – 1000	47 – 106	0.001 – 0.05

4.3 Ground-Penetrating Radar

4.3.1 Theory

GPR is a geophysical method used to determine variations in subsurface electromagnetic wave-propagation (Figure 3). The electromagnetic properties of materials are related to their composition and water content. These influence the velocity (v_m) of the radio wave propagation and its attenuation. Attenuation is the decrease in intensity of a wave as a result of absorption of energy (conversion of wave

energy into heat) and scattering (irregular dispersion of energy caused by homogeneities in the medium through which a wave is traveling) out of the path to the detector. This behavior depends on the speed of light c and fundamental material properties across the boundary such as the dielectric constant ϵ_r (for typical values see Table 1), and magnetic permeability μ_r . The permittivity, another name for the dielectric constant, measures the ability of a material to store a charge when an electric field is applied. It is given by $\epsilon_r = \epsilon/\epsilon_0$ which is the ratio of the dielectric permittivity of the medium to the dielectric permittivity of free space. Magnetic permeability on the other hand is a measure of the easiness to magnetize a medium when put in an electromagnetic field. It is the ratio between the permeability of the material divided by the permeability of free space. The velocity of the electromagnetic wave propagation is given by:

$$v_m = \frac{c}{\left(\frac{\epsilon_r * \mu_r}{2}\right) [(1+P^2)+1]^{\frac{1}{2}}} \quad (1)$$

Where P is the loss factor (ratio between the conductivity and the frequency of the submitted radiomagnetic wave times the permittivity, $P = \sigma/\omega\epsilon$). Most soils and sediments are only slightly magnetic and have low magnetic permeability (Burger et al., 2006). Furthermore, GPR signals are high-frequency, which leads to an assumption $\sigma \ll \omega\epsilon$ (called the wave regime approximation) and thus $P \rightarrow 0$, which simplifies equation (1) into:

$$v = \frac{c}{\sqrt{\epsilon_r * \mu_r}} \quad (2)$$

For most geological materials, which are saturated in water, this propagation velocity is going to be low because its dielectric permittivities are high. Dry rocks and igneous rocks have higher propagation velocities.

4.3.2 Measurement procedure

In this study we used the Geophysical Survey Systems, Inc (GSSI) GPR equipment, owned by Empresa Pública Metropolitana de Agua Potable y Saneamiento de Quito (EPMAPS) (Figure 4). The system consists of a SIR-3000 control unit and accessories and the sending and receiving antenna with either 200 MHz or 400 MHz central frequency (Geophysical Survey Systems, 2014, 2017). The antenna sends the electromagnetic waves and collects the returning signal. The control unit computes the two-way travel time which can be further converted to a depth estimate by assuming certain soil type. The depth in reflection profiles can be determined based on: (1) the travel time of the signal and (2) electromagnetic parameters of the emitted waves (Figure 3).

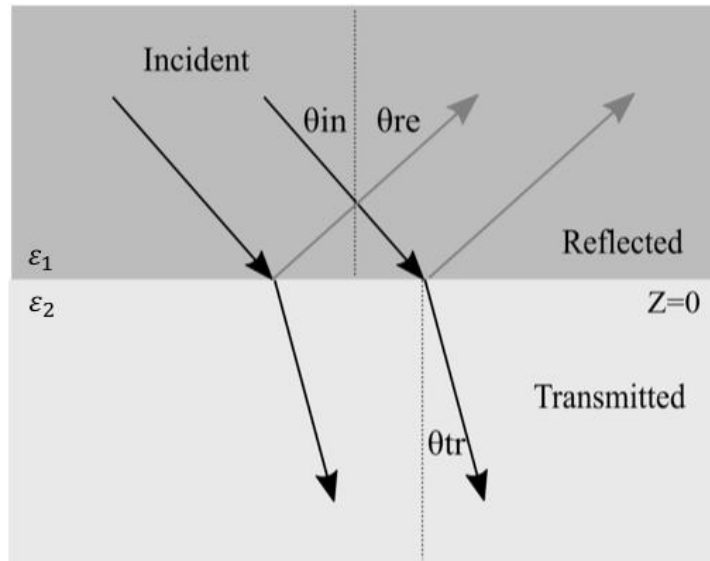


Figure 3. Simple sketch of the propagation of electromagnetic waves at an interface. A horizontally polarized plane electromagnetic wave encounters obliquely a planar interface separating two lossless dielectric media where E is the electric field, H is the magnetic field vector, \hat{p} is the propagation vector, \hat{q} the reflection vector, θ_i is the incident angle, θ_r is the reflected angle, θ_t is the transmitted angle, ϵ_1 is the dielectric constant. Modified after Everett (2013).

We preferred the lower frequency antenna due to better penetration depth, however due to technical difficulties in 2017 all but survey line B-B' was measured with the 400 MHz antenna (Table 2). In the field, we use the control unit to configure the antenna, calibrate the survey wheel for distance, and set the viewing depth, soil type and unit of measurement (Geophysical Survey Systems, 2014). Then, we pass over the established survey line by dragging the antenna and the control unit across it (Figure 4).

Table 2. Acquisition of information for the GPR survey lines (See Figure 2 for location).

Location	Date	Length (m)	Depth (m)	Antenna (MHz)
A - A'	11-2017	96	~6	200
A - A'	11-2017	96	~3.5	400
B - B'	11-2017	96	~3.5	400
B - B'	11-2017	96	~3.5	400
A - A'	11-2018	118	~ 6	200
A - A'	11-2018	118	~ 6	200
B - B'	11-2018	125	~ 6	200
B - B'	11-2018	125	~ 6	200

In November 2017 we did three GPR profiles: two perpendicular (SN) to the slope of the hill and one parallel (WE). The first perpendicular line A-A' was up slope from the pond and the second B-B', below. The third survey line, parallel to the slope, did not

provide us additional information and was not repeated in the November 2018 GPR surveying. The third parallel survey line done in 2017 is therefore not discussed further. Each year the GPR surveys were done both from A to A' and back (same case for B to B'). This results in four radargrams per year. The opposite directions were done in order to check for repeatability.



Figure 4. GPR equipment of EPMAPS in the field. Diego Guanotuña is holding the control unit in his hands on the left of the photo. The main sending/receiving antenna is in the orange box being pulled by Gustavo Béjar (right). The box is connected to a survey wheel which simultaneously measures the distance.

The data were processed using a software called RADAN 7. The processing steps for each radargram started with the time zero setting to regulate the vertical position of the entire profile in the data frame. It gives a more precise depth calculation because it sets the top of the scan to a near estimate of the ground surface, thereby removing the layer of air in between the GPR and ground. Then, we did the background removal, which is a filter that eliminates horizontal bands of noise that can be produced by low frequency noise such as antenna ringing. If not removed, it can hide existing horizontal reflectors. Then, we applied a filter that improves the quality of the radargram considering the background noise. The color scale was adjusted to best show the

contrast in our data. Finally, when the radargram was ready, we exported the entire file as a PNG image.

4.4 Electrical Resistivity

4.4.1 Theory

The ERT method is based on how materials oppose the flow of a current. It is an active geophysical method and requires inducing an electric field and therefore a current flow in the ground. The dynamics of electric current and electric field driven by variations in the subsurface materials cause changes in the electric potential V and the current I . To understand how the resistivity method is used to estimate Earth resistivity, think of a cylindrical sample of certain material with length L [m], resistance R [Ω] and cross-sectional area A [m^2]. Knowing that the resistance of a material is proportional to the length and inversely proportional to the cross-sectional area, we obtain the following equation:

$$R = \rho \frac{L}{A}, \quad (3)$$

where ρ [units of $\Omega \text{ m}$] is the resistivity of the material. The reciprocal of this physical property is the electrical conductivity, denoted σ [units of S/m]. As the current I is proportional to the potential difference V across it:

$$V = IR, \quad (4)$$

by substituting equation (3) in equation (4) we obtain:

$$\frac{V}{L} = \rho \frac{I}{A}. \quad (5)$$

The ratio V/L is the electric field E (assuming the potential gradient to be constant along the length of the conductor). The ratio I/A is the current per unit cross-sectional area of the conductor which is also called the current density and denoted J . Rewriting the Ohm's law (4) we obtain:

$$E = \rho J. \quad (6)$$

Considering that the electric field lines are parallel to the current flow and normal to the equipotential surfaces, that are hemispherical in shape, the current density J is equal to the current divided by the surface area for a hemisphere of radius r (which in the case of ground will be half the surface of a sphere $4\pi r^2/2$). Now, in the case of homogeneous ground we obtain:

$$E = \rho J = \rho \frac{I}{2\pi r^2}. \quad (7)$$

In this study, we applied the electrode configuration of Frank Wenner (Weimer, 1916; Figure 5a) which has a high vertical resolution for horizontally layered media. For this array, all electrode separations have the value a , and the geometric factor K is computed by multiplying by $2\pi a$. Therefore, for the Wenner array the apparent resistivity is:

$$\rho_{app} = \left(\frac{V}{I}\right) K = \left(\frac{V}{I}\right) 2\pi a, \quad (8)$$

where V is the voltage drop between the potential electrodes (P1 and P2), I the current and a the spacing between each electrode. The two outer electrodes (C1 and C2) are connected to an ammeter, which measures the current. The two inner electrodes are connected to a voltmeter which measures the voltage [V or mV]. The vertical depth profile of the different resistivities of the subsoil is found by increasing the value a and conserving the location of the center point of the array. By moving the electrodes to one side across the surface and maintaining a constant, we obtain the horizontal profile (Herman, 2001).

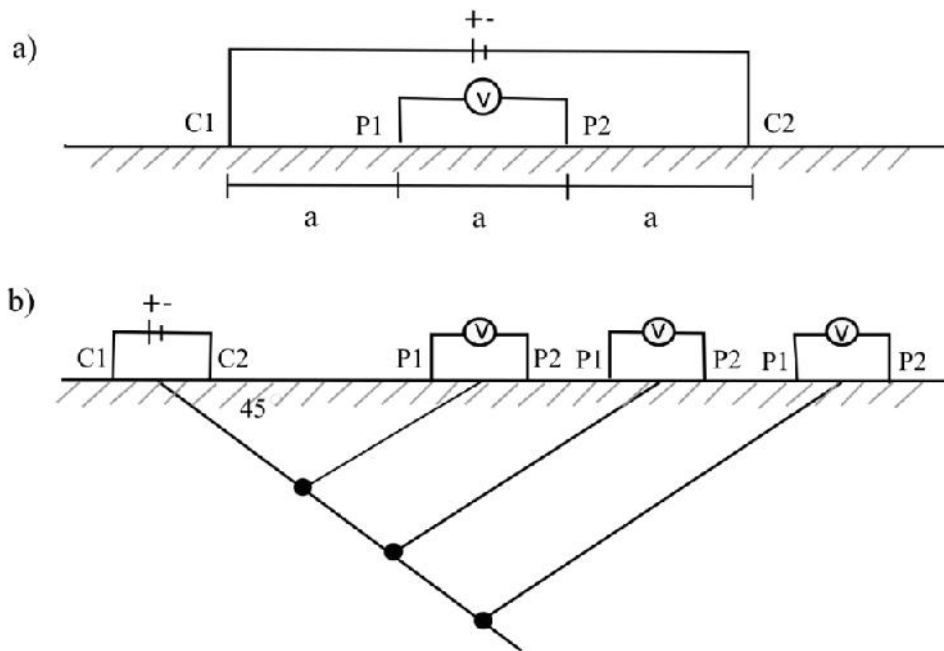


Figure 5. Sketches of the two electrode configurations used in this study. a) Wenner electrode configuration. C1 and C2 are the electrodes connected to the battery that creates the current. P1 and P2 are the electrodes reading the voltage in Volts. b) Dipole-dipole electrode configuration. Furthermore, this sketch shows how the consequently deeper depth (apparent depth) is gained for the apparent resistivity estimate by measuring the potential stepwise further and further away from the current electrodes.

4.4.2 Measurement procedure and data analyses

In order to acquire the data, we built electrical resistivity tomography equipment based on the works of Herman (2001) and Clark & Page (2011) (Figure 6). Electrical resistivity surveys were planned to determine the resistivity distribution in the subsurface of the area near the pool. In November 2017, using the Wenner array, we did two geoelectrical profiles perpendicular to the slope, exactly where the GPR profiles were recorded. They are also called A-A' and B-B' and have an initial electrode spacing of 1m. The approximate reached depth for these surveys is about 3.5 m.

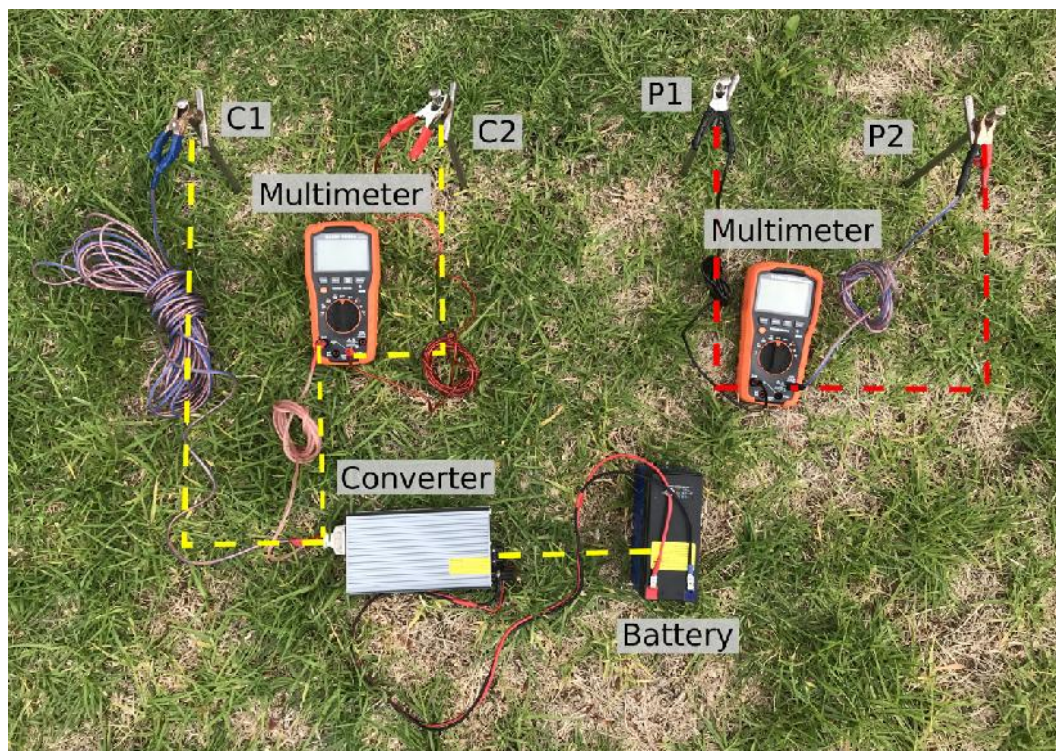


Figure 6. Photo of the ERT equipment used for obtaining the data following dipole-dipole electrode configuration. The electrodes C1 and C2 are connected to a multimeter (measuring the current) and through an electricity converter to a battery. The electrodes P1 and P2 are connected to another multimeter to read the potential.

In September 2018 we repeated the Wenner array surveys along A-A' and B-B' in order to see the changes of the resistivity in the subsoil in comparison with one year ago. From October 2018 to February 2019 we applied the dipole-dipole configuration (Table 3), each month, to create a time-line of the resistivity changes. Additionally, in February the profiles were also measured from A' to A to control for the effects arising from the travel direction of the survey. In total, 14 geoelectrical surveys were completed with a 4 m dipole electrode spacing up to a separation L of 44 m. This permitted us to reach a depth of about 11 m, about three times as deep as in December 2017.

Table 3. – Data of each ERT survey line. W: Wenner, DD: Dipole-Dipole (See Figure 2 for location).

Location	Date	Length (m)	Depth (m)	Array
A - A'	11-2017	48	2.62	W
B - B'	11-2017	87.1	2.62	W
A - A'	09-2018	81	3.13	W
B - B'	09-2018	40	3.13	W
A - A'	10-2018	100	11.5	DD
B - B'	10-2018	104	11.5	DD
A - A'	11-2018	100	11.5	DD
B - B'	11-2018	100	11.5	DD
A - A'	12-2018	100	11.5	DD
B - B'	12-2018	100	11.5	DD
A - A'	01-2019	100	11.5	DD
B - B'	01-2019	100	11.5	DD
A - A'	02-2019	100	11.5	DD
A' - A	02-2019	100	11.5	DD
B - B'	02-2019	100	11.5	DD
B' - B	02-2019	100	11.5	DD

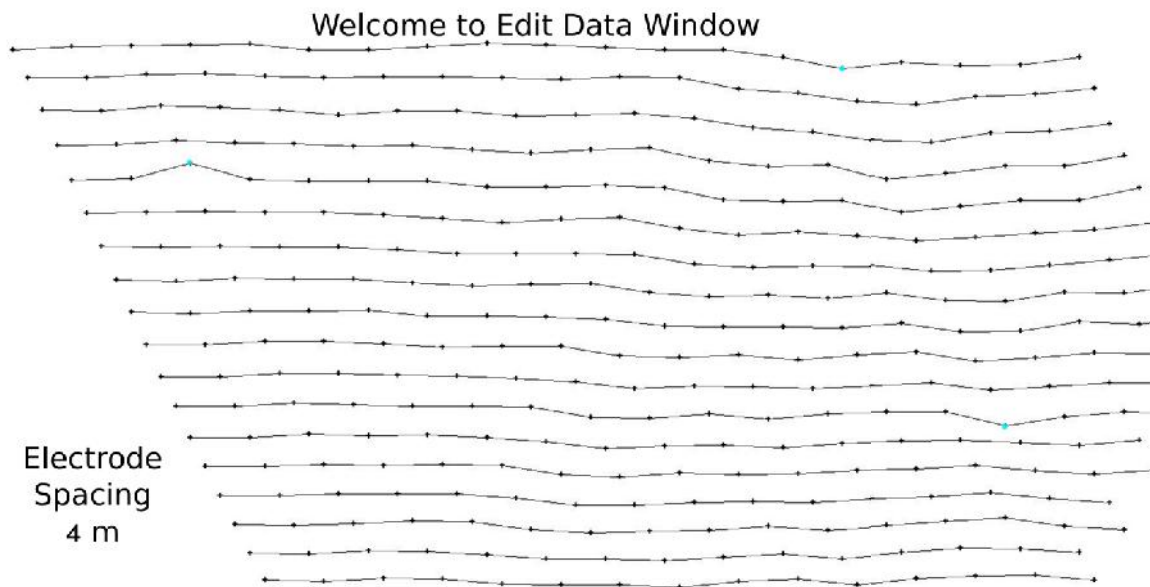


Figure 7. Data points acquired in the field viewed by the RES2DINV computer program for erroneous data points analysis. Each point represents a subsurface measurement point (see Figure 5b). The sky-blue dots are the points selected to be eliminated.

The acquired ERT data was processed with the RES2DINV program, which determines a two-dimensional resistivity model for the subsurface data obtained from 2-D electrical imaging surveys (Geotomo Software SDN BHD, 2018). After acquiring the data in the field (readings of current and potential difference with varying electrode

distances) we calculated the apparent resistivities with equation (8) for the Wenner array and equation (9) for the dipole-dipole array.

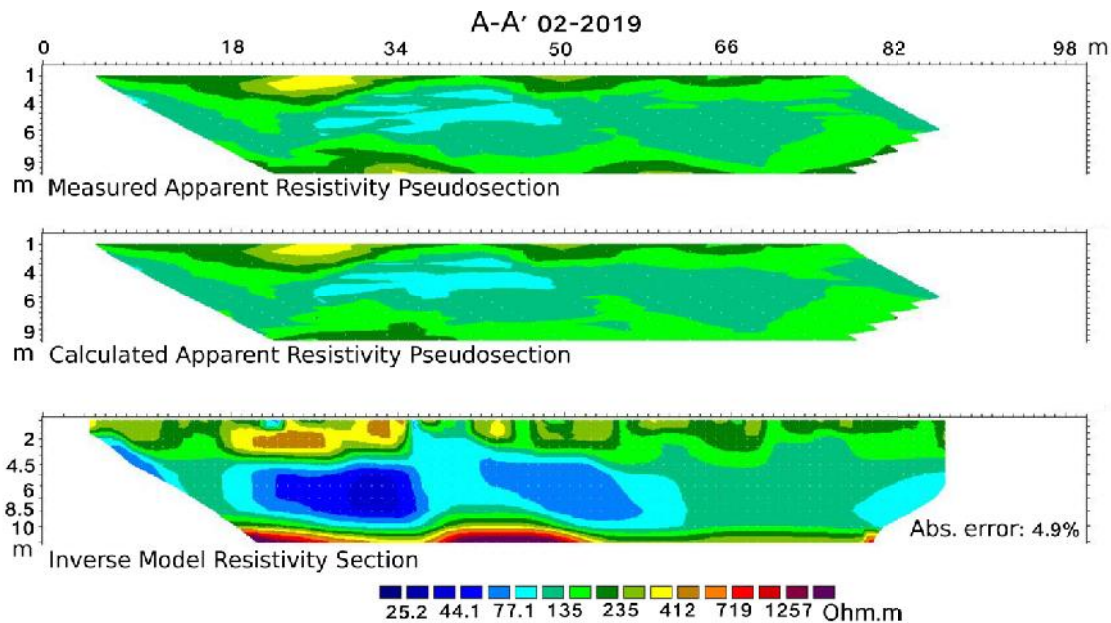


Figure 8. Two pseudosections and the model data of survey line B-B' below the pool in January 2019. The first diagram shows the actual measured values of resistivity in a pseudosection. In the second diagram are plotted the calculated values, also in a pseudosection and the third diagram is the new model of the subsurface based on four iterations. The root-mean-square (RMS) error between the resistivity pseudosection calculated based on the model (the second diagram) and the actual measured resistivity pseudosection (the first diagram) is 5.2%.

Before uploading the data to RES2DINV, plots of apparent resistivity vs distance were performed to initially check for erroneous datapoints, which were either removed or corrected (in case of the error being wrong units, for example). In the RES2DINV we further viewed all the data points (Figure 7) and removed other erroneous points that we had not noticed during our initial error analysis. After the data was clean of obvious error points, we ran the inversion and obtained two pseudosections and a model (Figure 8). The first pseudosection represents the actual measured apparent resistivities. The second provides the calculated apparent resistivities based on the iteration model. The last is the inverse model section of what might be the actual resistivity values of the subsurface that could cause the apparent resistivities. The inversion is based on a finite-difference modelling subroutine, that calculates the apparent resistivities and uses a non-linear smoothness-constrained least-squares optimization method to calculate the resistivity of the model blocks. The blocks are rectangular, loosely tied to the distribution and amount of the data points in the pseudosection (deGroot-Hedlin & Constable, 1990). The optimization method works by trying to reduce the difference between the calculated and the measured apparent resistivities by changing the resistivity of the model blocks under the smoothness

constraints given by the user. That difference is given throughout the inversion process and provided in the results as the root-mean-square (RMS) error (e.g. Figure 7).

We also applied the model refinement (Figure 9). By default, the RES2DINV program uses a model where the width of the interior model blocks and the unit electrode spacing is the same. It is useful in most cases but not when there are large variations of resistivity near the surface and especially for dipole-dipole data, which is more sensitive to this (Geotomo Software SDN BHD, 2018). For these cases, the model refinement will increase the amount of model blocks, which can allow for a better fitting of the data. For this work, we chose the width of the model cells to be half the unit electrode spacing.

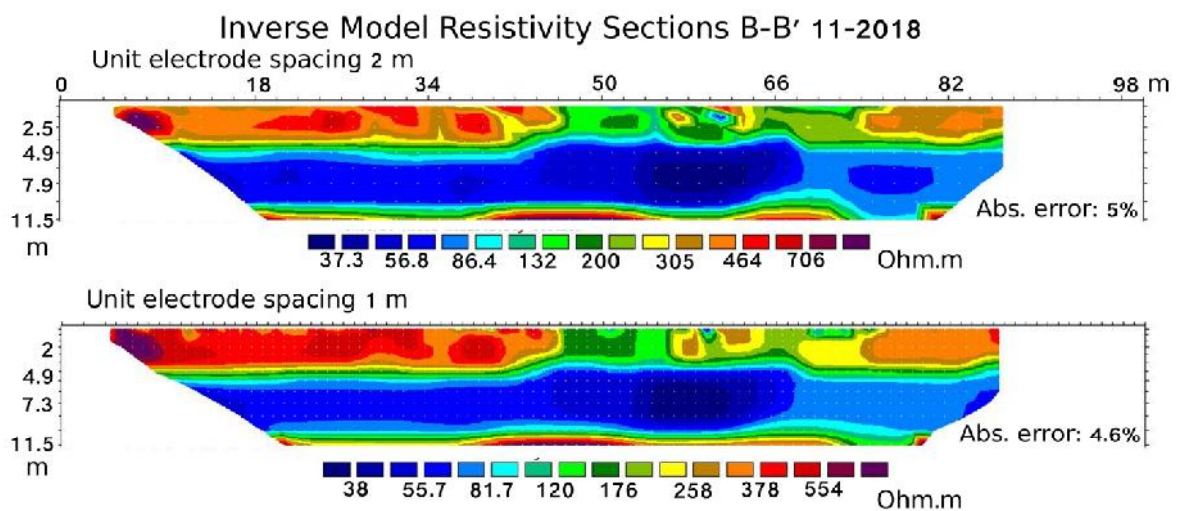


Figure 9. Two inversion models for upper survey line A-A' in November 2018 with different model parameters. The model at the top uses electrode spacing as the model block size. The model at the bottom is refined, that is the amount of model blocks is increased, which can allow better fitting for data with large variability in the resistivity values between neighboring data points. The values of resistivity changes also change with the refinement.

All the inverse models were created using four iterations because the demo version of the computer program is limited to four iterations. Nevertheless, in general, a good approach to select a suitable model is to stop in an iteration in which the RMS error does not vary considerably and the RMS error is less than 10% (Geotomo Software SDN BHD, 2018). Usually, these values appear from 3 to 6 iterations but in this study, 3 to 4 iterations were typically enough. If more iterations are performed, there will not necessarily be significant changes in the inverse model and the improvement in fitting the model to data can actually occur through over-complicating the existing geology.

For all the pseudosections and inverse models, we established a contour interval for the resistivities in order to better compare monthly variations. Finally, to establish the topography profile for the survey lines, we used the DJI Inspire 2 drone to take a set of aerial pictures of the area where the pool is located (Figure 10 and Figure 21) in order to create a Digital Elevation Model (DEM). The aerial pictures were taken closely

spaced (minimum of 70% of overlap), which allowed us to create a high-resolution 3D model of the survey area in the free WebODM Drone Software (Figure 10). The topography of each survey line was then estimated from this 3D model and are included in each ERT model.

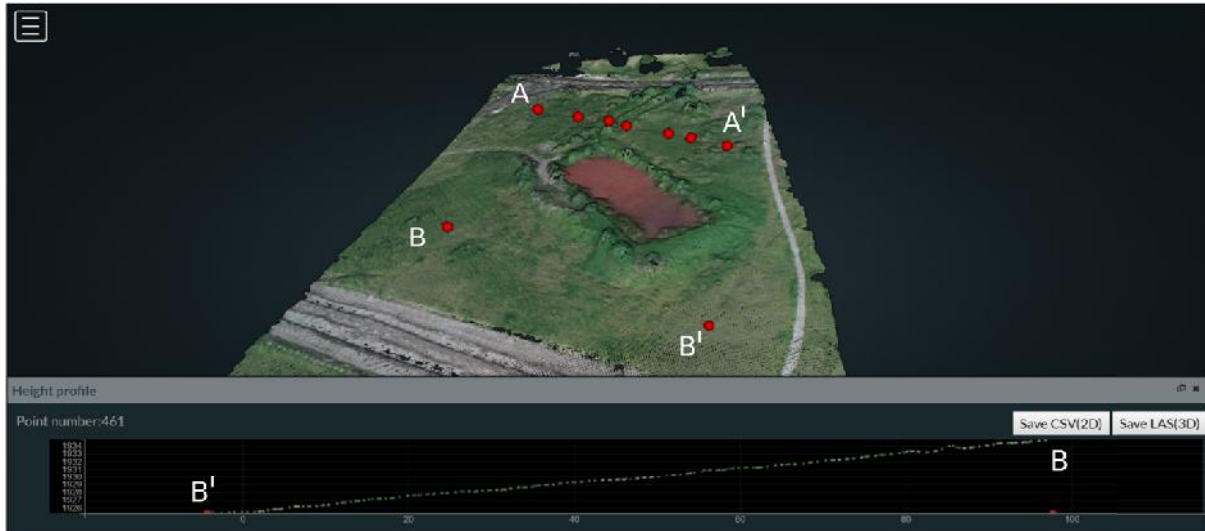


Figure 10. Photos of the WebODM desktop program for obtaining the topography of the survey lines. The top image is the 3D point cloud, that is a set of data points in space that measure the distance to external surfaces of objects, and represents a digital elevation model. On the bottom is the height profile of the survey line B'-B, that was used for obtaining topography of that survey line.

5 RESULTS AND DISCUSSION

5.1 Stratigraphy of the area

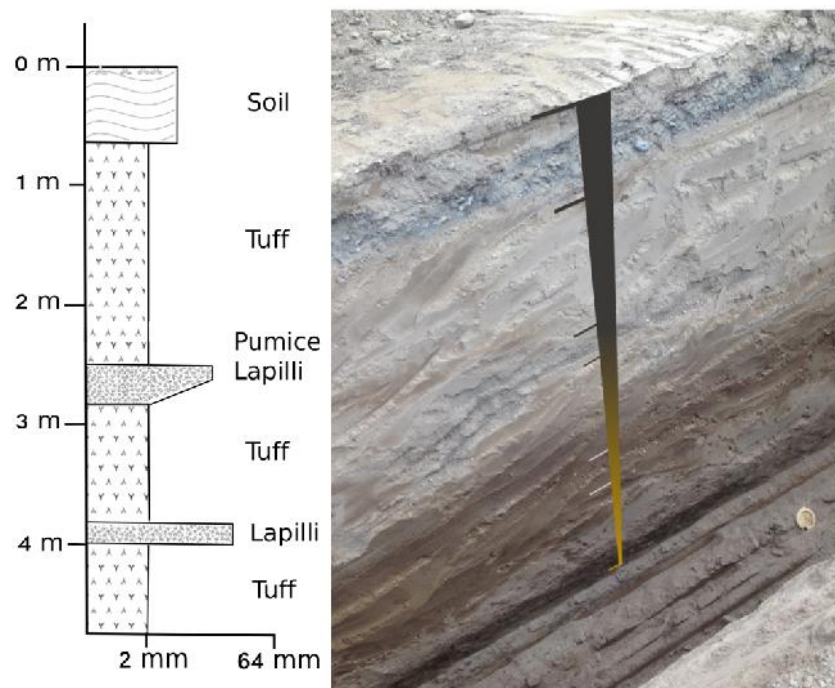


Figure 11. Representative stratigraphy of the first ~5 m of the subsoil in the study area at Point 1. On the left is a stratigraphic column of the outcrop, shown on the photo on the right. For locations see Figure 1.

We analyzed the stratigraphy from two outcrops, each approximately 5 m deep, located near the study area. Because both outcrops show the same stratigraphy, we present only one location (Figure 11). We documented the stratigraphy from top to bottom. The first layer is soil covered by medium vegetation with plenty of roots. Below, 4 m of intercalations of brown fine tuff and pumice lapilli. The first ~80 cm is a thick matrix-supported bed of pumice lapilli with lapilli sizes ranging from 0.3 cm to 2 cm. Its contacts are transitional and graded from fine to coarse and again to fine. The second bed of lapilli is separated from the first one by 1.5 m of tuff. This bed does not have matrix and is well sorted. Its inferior contact is sharp while the superior is transitional and normally graded. At approximately 3 m deep, moisture can be seen darkening the color of the tuff.

5.2 Water Biophysicochemical Analysis

Water samples were sent to Laboratorio Lasa S.A Quito for biochemical analysis. The pH, conductivity and total suspended solids were measured at Yachay Tech. The testing methods and results are specified in Table 4. In order to determine if the water that is arriving to the pool is contaminated with organic material, we used *Table 1. Compounds that affects potability, Table 4. Chemical compounds pollution indicators,* and *Table 5. Bacteriological quality* presented in the Ecuadorian Practice Code CPE INEN 5 Part 9-1:1992 (de Construcción, 1992), and information from App4water, 2019; Blog, 2017; Mallon, 2017.

Table 4. Physicochemical analyses and properties of water samples from the study area. The first two analyses (BOD and NTK) were done by 02/2019 and the rest (pH, conductivity and total suspended particles) by 05/2019. See Figure 2 for locations.

Parameter	Max acceptable concentration for drinking water	Minimum concentration for wastewater	Location 1	Location 2	Location 3	Unit
BOD	6	100	7.30	12	1.46	mg/L
NTK	1	20	6.44	4.74	5.86	mg/L
pH	8.5	6.5	7.41	8.63	8.62	pH units
Conductivity	1000	800	134.5	136.7	137.1	uS/cm
TSP	1500	100	30.5	36.6	30.5	mg/L

The biochemical indicator, BOD, shows poor water quality in locations 1 and 2, corresponding to the water located in the pool and at the incoming channel connected

to it. This signifies that there is organic matter present in the water and that microorganisms are decomposing that organic matter/waste (Ias, 2015). The water at location 3 has a value of 1.4 mg/L, indicating good quality. The three samples show nitrogen in quantities ranging from 4.7 to 6.4 mg/L. This indicates that there is a low percentage of feces and urine, but in any case, these amounts are too high for drinking water. Also, the presence of nitrogen can facilitate eutrophication, especially in the pool where the water stagnates. In this thesis, we identify the algae present on the surface of the pool (Figure 12) with *Azolla* algae because of its physical similarities and functions. Indeed, this alga is used to feed animals due to its high content in proteins and minerals. Also, it is used in rice crops due to its capacity to fix nitrogen and inhibit the growth of other plants. In the same way, as it covers all the water surface, it does not allow mosquitos to lay their eggs in the water. These algae together with pH and temperature affects the function of enzymes and amount of CO_2 in the atmosphere. The pH values for locations 2 and 3 are 8.6, while the pH in the pool is 7.4 where most microorganisms do well. Values for total suspended solids, which is a factor that affects potability, are relatively low. Suspended solids determine the color of the water which is also a marker of healthy or unhealthy water. On the other hand, the values of coliforms, bacteriological quality (Table 5), shows that the water is not suitable for human consumption. However, the values are way below the threshold for calling the water wastewater.



Figure 12. Collage of photos showing the pool and the algae. The photo on the left shows the details of the physical characteristics of the algae present on the surface of the pool, similar in appearance with commonly found *Azolla*. The photo on the top right represents how the pool looked like in 09/2018. The photo on the bottom right shows how the algae grew by 11/2018.

In summary, the biophysiochemical water analyses prove that the water sampled in the pool, in the portion of the acequia that is supplying water in the pool and the portion of acequia that is transporting the water from uphill, is not suitable for human consumption. This is specifically due to the amount of coliforms present, total nitrogen

and, BOD. However, the water does not meet the criteria for wastewater itself. For these reasons, we can say that the water from the acequia is contaminated in low percentage while flowing to Yachay. Use for agriculture is, on the other hand, completely safe.

Table 5. Bacteriological Quality (de Construcción, 1992) and measured values of samples from this study.

Classification	NMP/100 ml of Bacteria Coliform	Location	Measured value [NMP/100ml]
Requires only disinfection treatment	0 – 50	1	65×10^3
It requires conventional methods of treatment.	50 – 5 000	2	11×10^4
Intense pollution that forces more active treatments.	5 000 – 50 000	3	77×10^3
Very intense pollution that makes water unacceptable unless it resorts to special treatments.	More than 50 000		

5.3 Ground-Penetrating Radar

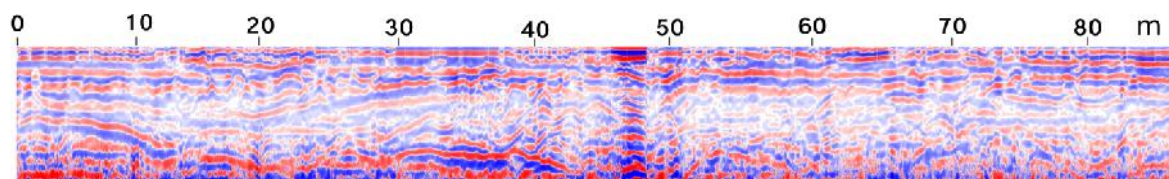


Figure 13. Radargram showing A-A' survey line (See Figure 2 for location). The zones where the colors are intense show more content of water or moisture. The zones where the colors are weak are dryer. The apparent depth is 5 m approximately.

Data were acquired on both survey lines twice: from S to N and vice versa for comparison and in order to assure the data is reliable. The radargrams from 2018 for A-A' (Figure 13) are 100 m long. It shows zones with more reflectance at the bottom, which can be compared with the beginning of moisture present in Figure 11. High reflectance is also observed at the top where the infiltration of superficial water and sub-superficial water is flowing. The vegetation at the surface is apparent where humidity is higher. Around 44 m distance, a significant discharge of water occurred during the month of GPR data collection, November 2018. Consequently, the radargram shows a high reflectance along a vertical area. The radargram of survey line B-B' is shown in Figure 14. It is 100 m long. Unlike the first radargram, this survey line shows a more defined subsurface. It means that there is not much variation in the soil which allows us to more easily recognize the humid areas. We can see that in general, this area is dryer at the top and only deeper zones have high reflectance.

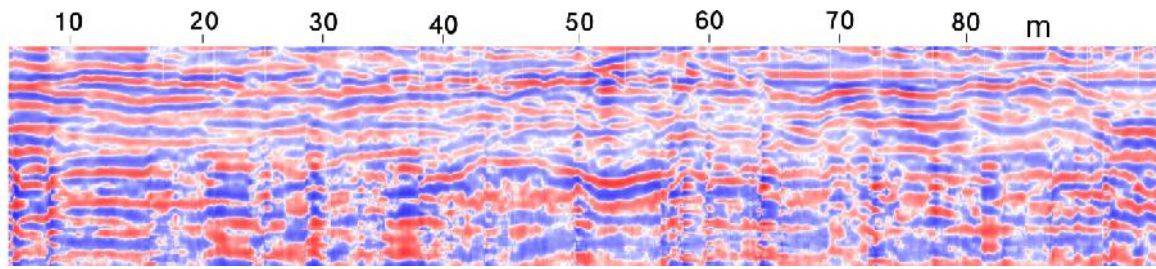


Figure 14. Radargram showing B-B' survey line (See Figure 2 for location). The zones where the colors are intense show more content of water or moisture. The zones where the colors are weak are dryer. The apparent depth is 5 m approximately.

5.4 Electrical Resistivity

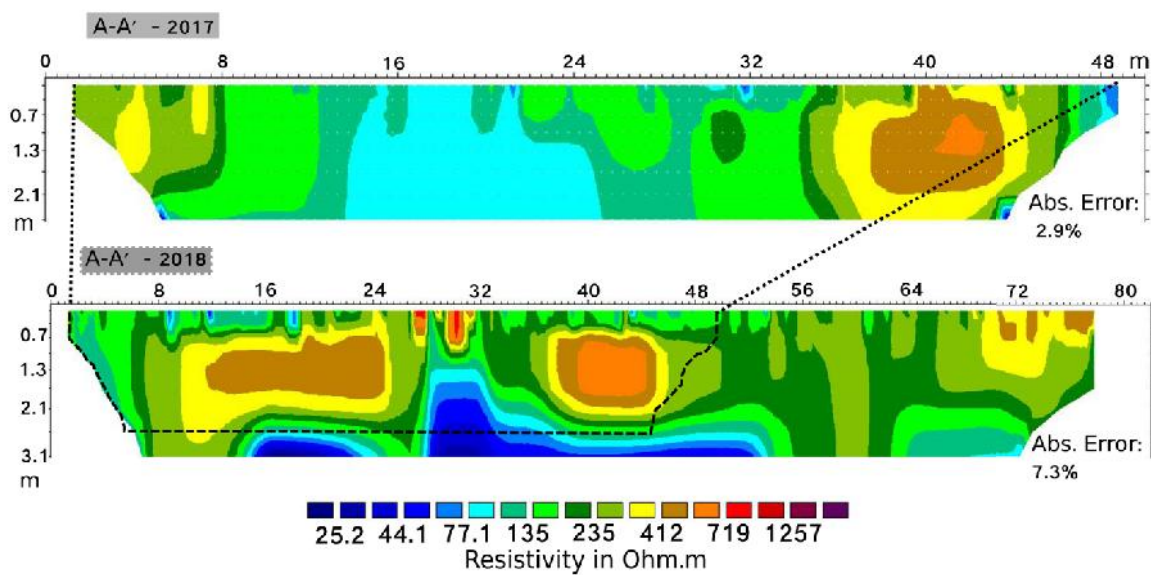


Figure 15. ERT inverse models for A -A' (See Figure 2 for location). Both survey lines were taken with the Wenner array. The top image is from 12/2017. The bottom image corresponds to 09/2018. The dashed lines are the area covered by the inverse model of 2017. The survey line of 2018 is longer and deeper.

The 50 m long and 2.6 m deep resistivity model along line A-A' from November 2017 obtained with the Wenner array shows resistivity values from 77.1 Ωm to 412 Ωm . It presents higher resistivity values at the edges, especially on the right side. The center is more conductive, matching with the green vegetation patch depicted in Figure 2. The other resistivity model below the pool (B-B') from the same year presents higher resistivities between 38 m to 90 m reaching up to 719 Ωm . A-A' and B-B' from September 2018 are 80 m long and 40 m long respectively. The data were not taken at the exact same coordinates as in 2017 but nearby. However, the resistivity patterns and values between the inversion models of these two years are similar (Figure 15). Nevertheless, considering that the irrigation ditch was not present in 2017, in 2018, the resistivity values of that area changed. It is important to point out that the weather in the second semester of 2017 was sunny and dry in general. According to Meteoblue

(2019), August 2018 was also a dry season with ~ 1.3 mm of precipitation and 4 mm as maximum precipitation in September 2018 in the middle of the month for one week (Figure 17). This confirms the similarity between the Wenner array pseudosections and inverse models even though the vegetation in 2018 has covered the dusty areas of 2017 (Figure 16).



Figure 16. Changes in vegetation over time in the study area. The photo of the left is from 2017 and the photo of the right is from 2018.

The ERT data from October 2018 and onward was obtained with the dipole-dipole electrode arrangement. The modelled resistivity inversions achieve a depth of ~11.5 m and a length of 100 m allowing us to have a larger view of the subsurface resistivity. For this set of data, we have to consider the newly dug water ditch located at 36-38 m of the survey line A-A' which appears as a semicircle of low resistivity (~135 Ω m) in the pseudosections and inverse models (Figure 20). The upstream line A-A' from October did not provide accurate information because its RMS error percentage is higher than 10%. This could be caused by problems with the equipment: water and salt water used to create better connection between the electrodes and the ground had gotten inside the cables causing severe rusting.

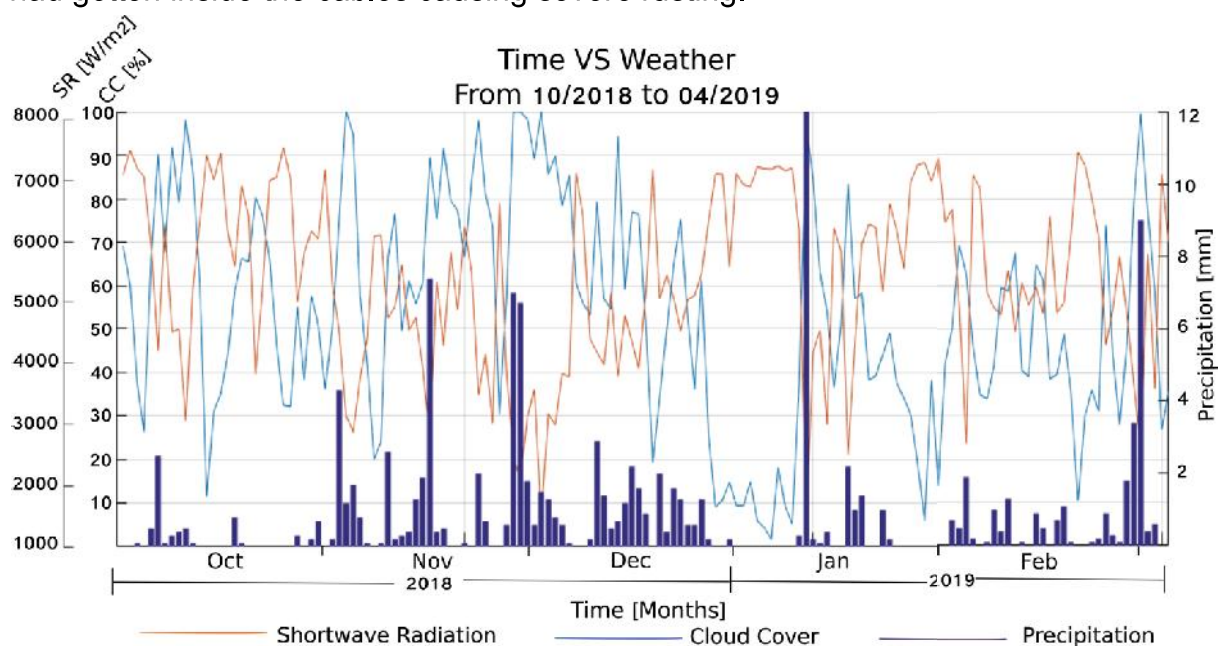


Figure 17. Plot time [months] versus precipitation [mm], cloud cover [%], and shortwave radiation [W/m²] from 08/2018 to 04/2019. Data obtained with the kind permission of Meteoblue (2019).

For this reason, this set of data will not be considered in the discussion. The downstream line B-B' (Figure 19) shows resistivity values from 25.2 Ω m to 1257 Ω m. The first 4 m below from the surface are characterized by high resistance especially on the left side. Between 5 and 11.5 m there is a zone with high values of conductivity especially at the bottom left and center. By this month, the maximum value of precipitation (Figure 17) is 2.5 mm but overall, it is also a dry month.



Figure 18. Photos showing the difference in vegetation due to the channel dug in November 2018. The photo on the left shows the half-way dug channel. The area below the dashed lines denote the abundant vegetation caused by this process. The photo on the right is in perpendicular direction with respect to the first photo. The area between the dashed lines also represents the abundant vegetation caused by the water that flowed from the channel.

A-A' from November 2018 (Figure 20) shows low values of resistivity from 25.2 Ω m to 235 Ω m. Values are especially low between 42 and 50 m due to an excavation nearby that generated an extra input of water in this area. This is noticeable also by the vegetation at the surface (Figure 18). The high conductivity zone in this month starts at 2 m depth. The resistivity of B-B' decreases compared with October 2018 (Figure 19). The precipitation for this month is frequent, around 16 days out of 30 (Figure 17).

In the same way, there is not a lot of sunshine days which can help in the evaporation of water. Therefore, the increase in conductivity of the soil for this month can be related with the intensification in precipitation (from 1 mm to 6 mm and ~ 15 mm by the end of the month).

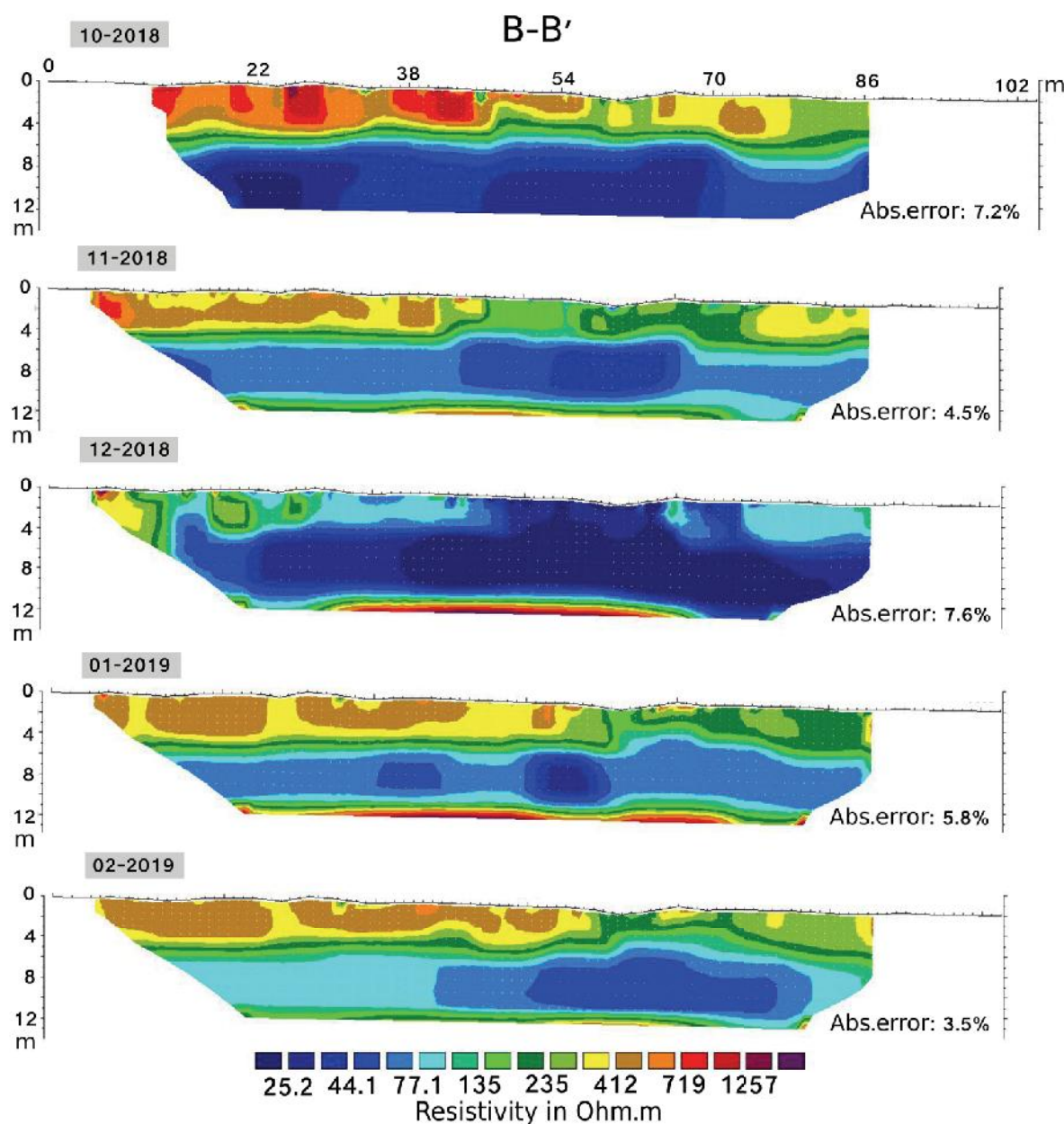


Figure 19. Scheme showing the changes in apparent resistivity from B-B' survey line (See Figure 2 for location) from October 2018 (top) to February 2019 (bottom). Low values of resistivity show areas with moisture while high values represent dry zones.

The upstream resistivities increased to 412 Ωm in December 2018 (Figure 20). Below 3.46 m the change is substantial from 25.2 Ωm to 44.1 Ωm while at the surface the change is not as marked. In contrast, the 2D pseudosection and inverse model B-B' (Figure 19) changes completely with respect to November 2018. Almost all the area turns very conductive, especially at the surface between ~40 and ~70 meters. It is also

obvious at the surface where the vegetation becomes thicker (Figure 18). The precipitation in this month is high (Figure 17). Out of 30 days about 23 were rainy days with values from 1 mm to 3 mm of water. The second half of the month presented some sunny days. The increase in resistivity for A-A' can be related with the fact that the values were taken in this period of time. The resistivity for B-B' can be related with the percolation of water from the top of the hill which appears in survey line A-A' in November 2019.

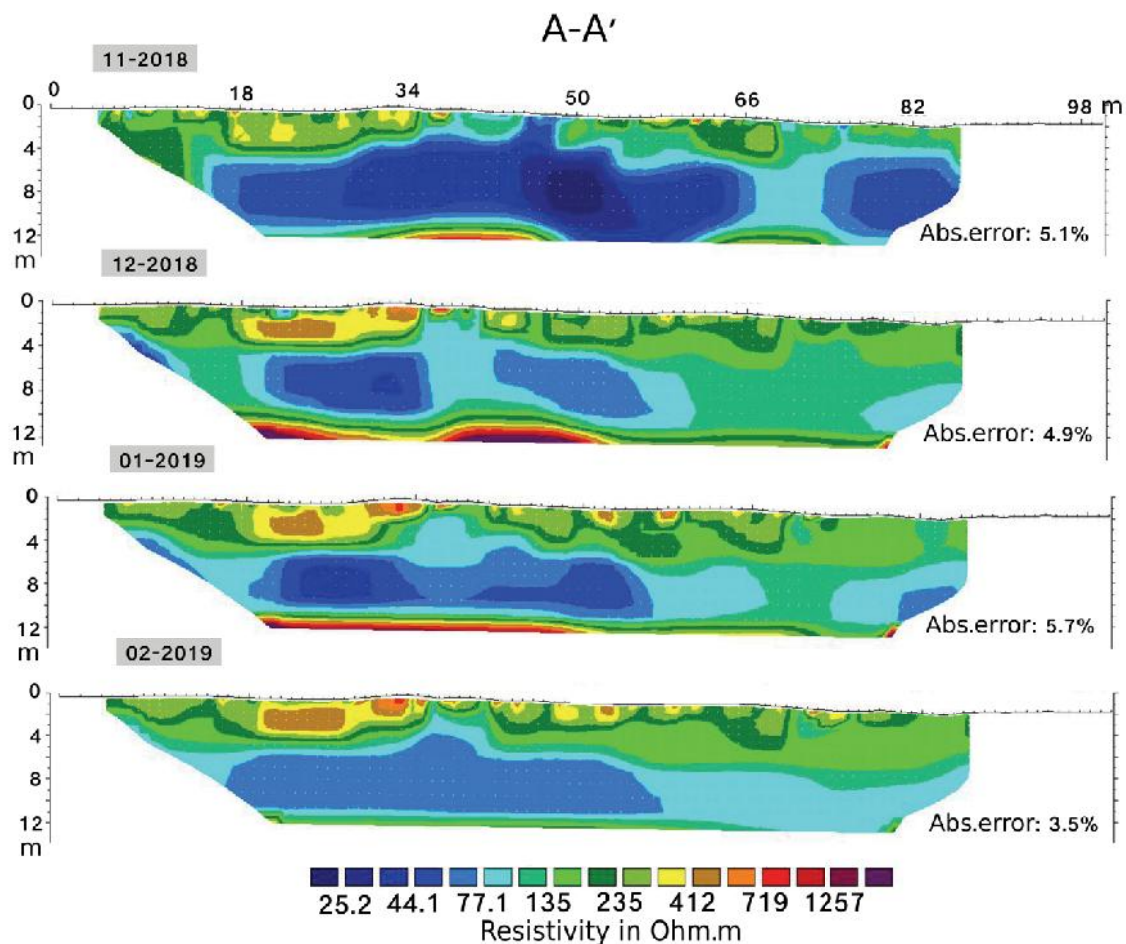


Figure 20. Scheme showing the changes in apparent resistivity from A-A' survey line (See Figure 2 for location) from October 2018 (top) to February 2019 (bottom). Low values of resistivity show areas with moisture while high values represent dry zones.

By January 2019, the profile A-A' shows a little increase in the resistivity especially at the surface. Deeper, the conductive area seems to expand. In contrast B-B', returns to the same values of resistivity (from 44.1 to 412 Ω m) as in November 2019. Precipitation for this month is almost nonexistent except for one day of rain with more than 10 mm of water. This can explain the general diminution of humidity in the subsoil.

Finally, the upstream line A-A' from February 2019 indicates the same behavior as the previous month except for the change in resistivity for the conductive zone from 44.1 Ω m to 77.1 Ω m. The same change is observed for the conductive area of B-B'

pseudosection. Additionally, in February, the pseudosections were also surveyed in reverse order A' – A and B' – B to confirm that the data is not severely affected by the direction of the surveying. Precipitation during this month is low (from 1 mm to 3 mm per day) which explains the reduction of values in the conductive zone.

We can affirm that the water content in the soil has changed with time in both lines A-A' and B-B'. We relate this to the channel dug that transports the water to the pool, the incomplete channel dug (Figure 18) and to weather conditions such as rainfall, cloudy sky and sunny days. We can clearly see in Figure 19 and in Figure 20 how the absence of rain and the increase of shortwave radiation changes the resistivity values and vice versa in at least the first couple meters depth. The extra input of water in November 2018 (Figure 20), makes the soil more conductive especially at the surface where the water flowed. This runoff plus the runoff of the precipitation traveling downhill appear in the model of December 2018 (Figure 19).

In general, the pseudosections and inverse model of A-A' survey line demonstrate that there is a bed of a resistant material ($\sim 412 \Omega\text{m}$) at the top followed by a more conductive ($\sim 135 \Omega\text{m}$) bed that gives way to a highly conductive layer (25.2 to 44.1 Ωm). We relate this with the presence of water in the soil at greater depths. Besides, the form of the vegetation patch of 2017 has changed with respect to 2019. The vegetation now joins the water channel that deposits the water into the pool, surrounds the pool and continues down the slope to the lower point of the pool, in the NE direction (Figure 21), giving the appearance that the water of the pool is being filtered.

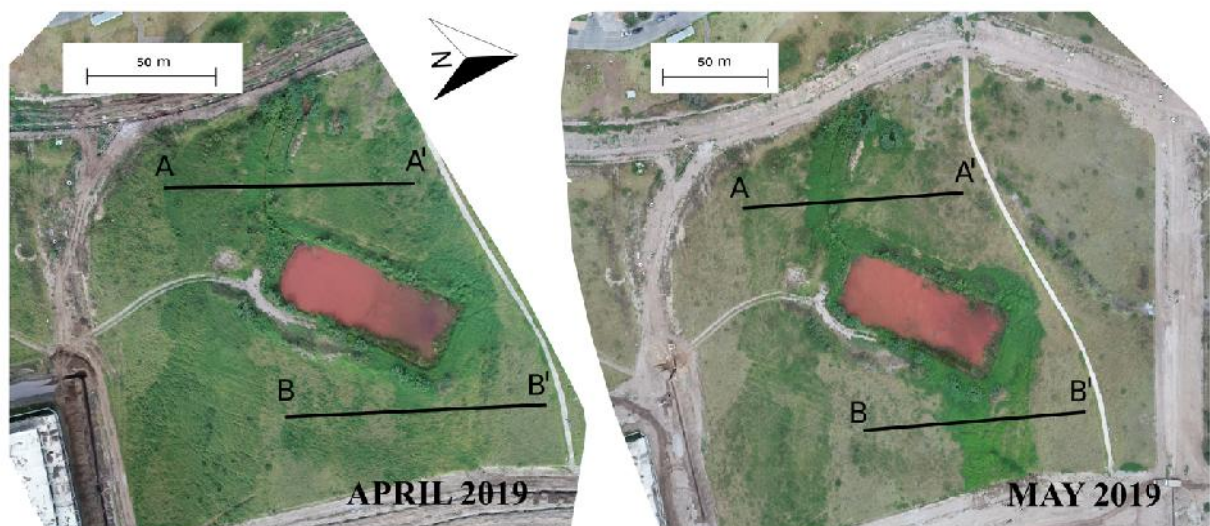


Figure 21. Aerial photos of the study area from April and May 2019. The photos show the change in the extent of the vegetation patch due to change of the water flow. The remain of the vegetation patch present in 2017 is at the left of the actual vegetation patch (May 2019).

Therefore, we can infer that now, the water is being channeled in its entirety and that the vegetation present in 2017 can now be seen as an old vegetation patch.

Furthermore, all the blue zone, which corresponds to low values of resistivity due to humidity below 4 m depth, is constant both in A-A' and B-B'. As at this depth is difficult to have big changes of water content, we suggest that this is due to the dipole-dipole array being sensitive to changes in the surface, which means that below 4 m depth, the changes in colors of the pseudosection are not necessarily real.

5.5 Comparison between ER, GPR and stratigraphy

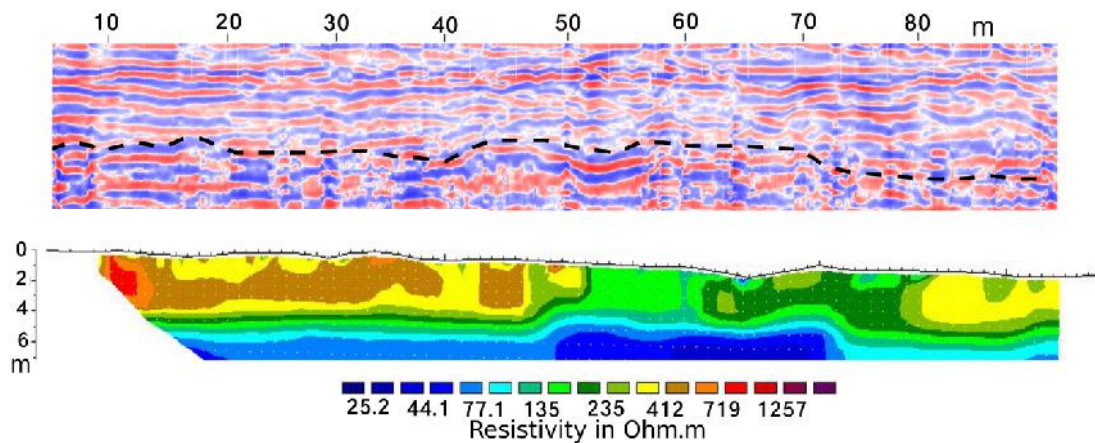


Figure 22. Electrical resistivity survey (bottom) from B-B' November 2018 and radargram (top). The dashed line separates the upper area that has low reflectance (low water content) from the lower area which shows higher reflectance (more water content).

In Figure 22 we can see that the subsoil is vertically well bedded. The dashed line in the radargram separates our interpretation of the dry zone (upper) from the more moisture containing zone (lower) which matches with the resistivity model of the same month. The blue color in the electrical resistivity model points out a conductive area, which in this case, is related with water content. In Figure 23, the areas with high reflectance at the surface matches with the vegetation patches while the areas at the bottom correspond to the humid areas seen in the stratigraphy in Figure 11. The extra superficial water flow in November 2018, due to the channel dug, is also shown in the radargram outlined by the vertical dashed line.

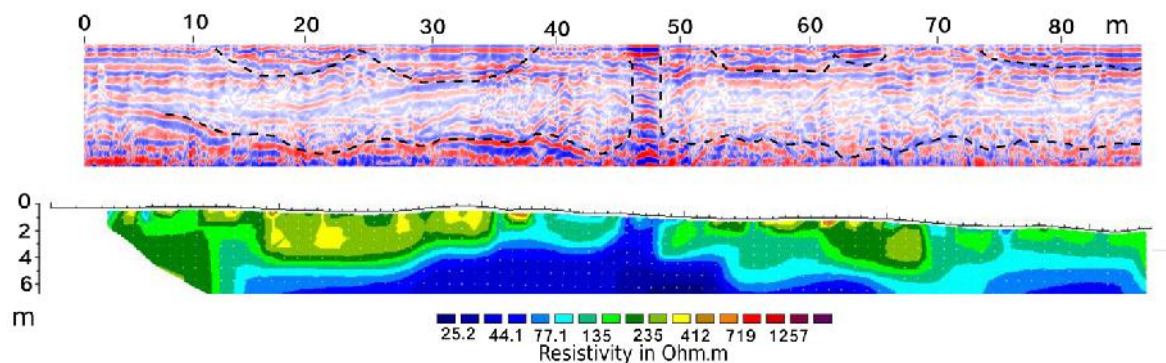


Figure 23. Electrical resistivity survey (bottom) from A-A' November 2018 and radargram (top). The dashed lines separate the areas of high reflectance from the areas with low reflectance. The former indicates the presence of moisture while the latter, dry areas respectively. High reflectance areas match with the vegetation at the surface and with the humid layer present in Figure 11.

6 CONCLUSIONS AND RECOMMENDATIONS

The results of the geoelectrical survey indicate that the first two meters of subsoil are sensible to changes in weather, specifically to rainfall, cloudiness and shortwave radiation. Beneath about three meters deep, the subsoil starts to turn more conductive. We relate this to the increase of moisture in the lithology (Figure 11). Currently, we can affirm that the channel that drives the water to the pool is depositing the water properly because the vegetation patch has changed (Figure 21). The vegetation follows the form of this channel, surrounds the pool and then continues to the lower zone of the pool indicating filtration of the water from the pool. This is also related with the direction of the flow which starts in the west and finishes in the northeast direction. Radargrams from the ground-penetrating radar confirm that areas with high resistivity and low conductivity are associated to moisture deep in the soil and moisture at the surface due to vegetation and runoff. Consequently, we confirm that the electrical resistivity equipment built based on Herman (2001) and Clark & Page (2011) obtain suitable data of subsurface structures.

Additionally, the water analyses show that the water collected from the acequias and the pool are not suitable for human consumption. Nevertheless, the values do not correspond to wastewater and therefore the water can be safely used for agricultural purposes. For further studies, we suggest to either build or buy a multichannel ERT equipment. Another interesting thing to try would be to use tracers to determine the velocity of the subsurface flow in order to compare with the changes from upslope to downslope. Lastly, to improve data quality with the dipole-dipole method it would be good to collect the monthly ERT survey data from A to A' and A' to A (as well as for B).

7 REFERENCES

- Abidin, M. H. Z., Baharuddin, M. F. T., Zawawi, M. H., Md Ali, N., Madun, A., & Ahmad Tajudin, S. A. (2015). Groundwater Seepage Mapping Using Electrical Resistivity Imaging. *Applied Mechanics and Materials*, 773–774, 1524–1534. <https://doi.org/10.4028/www.scientific.net/amm.773-774.1524>
- Adepelumi, A. A., Ako, B. D., & Ajayi, T. R. (2001). Groundwater contamination in the basement-complex area of Ile-Ife, southwestern Nigeria: A case study using the electrical-resistivity geophysical method. *Hydrogeology Journal*, 9(6), 611–622. <https://doi.org/10.1007/s10040-001-0160-x>
- Al-Fares, W. (2011). Contribution of the geophysical methods in characterizing the water leakage in Afamia B dam, Syria. *Journal of Applied Geophysics*, 75(3), 464–471. <https://doi.org/10.1016/j.jappgeo.2011.07.014>
- App4water. (2019). Characteristics of Wastewater. Retrieved from <https://www.app4water.com/characteristics-of-residential-wastewater/>
- Benson, A. K., Payne, K. L., & Stubben, M. A. (1997). Mapping groundwater contamination using dc resistivity and VLF geophysical methods—A case study. *Geophysics*, 62(1), 80–86. <https://doi.org/10.1190/1.1444148>
- Blog, T. W. (2017). Total Kjeldahl Nitrogen. Retrieved May 9, 2019, from <https://www.thewastewaterblog.com/single-post/2017/11/01/Total-Kjeldahl-Nitrogen>
- Bowling, J. C., Rodriguez, A. B., Harry, D. L., & Zheng, C. (2005). Delineating alluvial aquifer heterogeneity using resistivity and GPR data. *Ground Water*, 43(6), 890–903. <https://doi.org/10.1111/j.1745-6584.2005.00103.x>
- Burger, H. R., Sheehan, A. F., & Jones, C. H. (2006). *Introduction to applied geophysics: Exploring the shallow subsurface*. WW Norton.
- Cataldo, A., Persico, R., Leucci, G., De Benedetto, E., Cannazza, G., Matera, L., & De Giorgi, L. (2014). Time domain reflectometry, ground penetrating radar and electrical resistivity tomography: A comparative analysis of alternative approaches for leak detection in underground pipes. *NDT and E International*, 62, 14–28. <https://doi.org/10.1016/j.ndteint.2013.10.007>
- Clark, J. A., & Page, R. (2011). Inexpensive Geophysical Instruments Supporting Groundwater Exploration in Developing Nations. *Journal of Water Resource and Protection*, 03(10), 768–780. <https://doi.org/10.4236/jwarp.2011.310087>
- de Construcción, C. E. (1992). Normas para estudio y diseño de sistemas de agua potable y disposición de aguas residuales para poblaciones mayores a 1000 habitantes. *CPE INEN*, 5.
- deGroot-Hedlin, C., & Constable, S. (1990). Occam's inversion to generate smooth, two-dimensional models from magnetotelluric data. *Geophysics*, 55(12), 1613–1624.
- Dick, H. C., Pringle, J. K., Wisniewski, K. D., Goodwin, J., van der Putten, R., Evans, G. T., et al. (2017). Determining geophysical responses from burials in graveyards and cemeteries. *Geophysics*, 82(6), B245–B255. <https://doi.org/10.1190/geo2016-0440.1>
- Everett, M. E. (2013). *Near-surface applied geophysics*. Cambridge University Press.
- Feiger, N., Huss, M., Leinss, S., Sold, L., & Farinotti, D. (2018). The bedrock topography of Gries-A nd Findelengletscher. *Geographica Helvetica*, 73(1), 1–9. <https://doi.org/10.5194/gh-73-1-2018>
- Geophysical Survey Systems, I. (2014). Quick Start Guide. *MN72-448 Rev H*.
- Geophysical Survey Systems, I. (2017). SIR 3000 Manual. Geophysical Survey Systems, Inc.
- Geotomo Software SDN BHD. (2018). RES2DINVx64 ver. 4.08 User Manual.
- Herman, R. (2001). An introduction to electrical resistivity in geophysics. *American Journal of Physics*, 69(9), 943–952. <https://doi.org/10.1119/1.1378013>
- Huisman, J. A., Hubbard, S. S., Redman, J. D., & Annan, A. P. (2003). Measuring Soil Water Content with Ground Penetrating Radar: A Review. *Vadose Zone Journal*, 2(4), 476–491. <https://doi.org/10.2113/2.4.476>

- Ias, P. (2015). Biochemical Oxygen Demand. Retrieved May 9, 2019, from <http://prepareias.in/subject/gs/ecology-and-environment/-biochemical-oxygen-demand>
- Knapp, G. (1988). *Ecología cultural prehispánica del Ecuador* (Vol. 3). Banco Central del Ecuador Quito.
- Liu, Y., Shi, Z., Wang, B., & Yu, T. (2018). GPR impedance inversion for imaging and characterization of buried archaeological remains: A case study at Mudu city cite in Suzhou, China. *Journal of Applied Geophysics*, 148, 226–233. <https://doi.org/10.1016/j.jappgeo.2017.12.002>
- Mallon, E. (2017). Measuring EC (electrical conductivity) with Arduino. Retrieved May 9, 2019, from <https://thecavepearlproject.org/2017/08/12/measuring-electrical-conductivity-with-an-arduino-part1-overview/>
- Meteoblue. (2019). Descargar datos históricos 0.41°N 78.17°O. Retrieved May 9, 2019, from https://www.meteoblue.com/es/tiempo/archive/export/0.409N-78.169E2044_America%2FGuayaquil?daterange=2016-01-01+to+2019-04-30&locations=¶ms=¶ms%5B%5D=660%3Bsf¶ms%5B%5D=71%3Bsf¶ms%5B%5D=204%3Bsf&utc_offset=-5&aggregation=daily&temperature
- Park, S., Yi, M. J., Kim, J. H., & Shin, S. W. (2016). Electrical resistivity imaging (ERI) monitoring for groundwater contamination in an uncontrolled landfill, South Korea. *Journal of Applied Geophysics*, 135, 1–7. <https://doi.org/10.1016/j.jappgeo.2016.07.004>
- Ramirez, A., Daily, W., Binley, A., LaBrecque, D., & Roelant, D. (2009). Detection of Leaks in Underground Storage Tanks Using Electrical Resistance Methods. *Journal of Environmental and Engineering Geophysics*, 1(3), 189–203. <https://doi.org/10.4133/jeeeg1.3.189>
- Reynolds, J. M. (1997). *An Introduction to Applied and Environmental Geophysics*. <https://doi.org/10.1017/CBO9781107415324.004>
- Ribeiro, L. (2013). Machu Picchu: a civil engineering marvel. In 8. *Congreso Ibérico sobre Gestión y Planificación del Agua* (pp. 530–539). <https://doi.org/10.5860/choice.38-5410>
- Simyrdanis, K., Papadopoulos, N., Soupios, P., Kirkou, S., & Tsourlos, P. (2018). Characterization and monitoring of subsurface contamination from Olive Oil Mills' waste waters using Electrical Resistivity Tomography. *Science of the Total Environment*, 637–638, 991–1003. <https://doi.org/10.1016/j.scitotenv.2018.04.348>
- Sonkamble, S., Satishkumar, V., Amarender, B., & Sethurama, S. (2014). Combined ground-penetrating radar (GPR) and electrical resistivity applications exploring groundwater potential zones in granitic terrain. *Arabian Journal of Geosciences*, 7(8), 3109–3117. <https://doi.org/10.1007/s12517-013-0998-y>
- Soupios, P., Papadopoulos, N., Papadopoulos, I., Kouli, M., Vallianatos, F., Sarris, A., & Manios, T. (2007). Application of integrated methods in mapping waste disposal areas. *Environmental Geology*, 53(3), 661–675. <https://doi.org/10.1007/s00254-007-0681-2>
- Urish, D. W. (1983). The Practical Application of Surface Electrical Resistivity to Detection of Ground-Water Pollution. <https://doi.org/10.1007/s00254-007-0681-2>
- World Health Organization. (2006). *Overview of greywater management Health considerations: discussed and approved at the regional consultation on national priorities and plans of action on management and reuse of wastewater, Amman, Jordan*. WHO-EM/CEH/125/E [en línea]. Amman (Jordan): World Health Organization
-